StimDust: A 6.5mm^3, Wireless Ultrasonic Peripheral Nerve Stimulator with 82% Peak Chip Efficiency

Benjamin C. Johnson*, Konlin Shen*, David Piech*, M. Meraj Ghanbari*, Ka Yiu Li*, Ryan Neely*, Jose M. Carmena*, Michel M. Maharbiz*†, and Rikky Muller*†
*University of California, Berkeley, Berkeley, CA 94704, USA
†Chan-Zuckerberg Biohub, San Francisco, CA 94158

***Abstract*—We present a 6.5mm^3, 10mg, wireless peripheral nerve stimulator. The stimulator is powered and controlled through ultrasound from an external transducer and utilizes a single 750x750x750μm^3 piezocrystal for downlink communication, powering, and readout, reducing implant volume and mass. An IC with 0.06mm^2 active circuit area, designed in TSMC 65nm LPCMOS process, converts harvested ultrasound to stimulation charge with a peak efficiency of 82%. A custom wireless protocol that does not require a clock or memory circuits reduces on-chip power to 4μW when not stimulating. The encapsulated stimulator was cuffed to the sciatic nerve of an anesthetized rodent and demonstrated full-scale nerve activation *in vivo*. We achieve a highly efficient and temporally precise wireless peripheral nerve stimulator that is the smallest and lightest to our knowledge.**

***Index Terms*—Stimulation, neuromodulation, peripheral nerve, ultrasound, backscatter, low-power wireless**

I. Introduction

Peripheral nerve stimulators (PNSs) have shown promise in the symptomatic treatment a variety of disorders such as chronic pain, sleep apnea, incontinence, and arthritis [1], [2]. A primary technological barrier to widespread adoption of peripheral nerve stimulators is the need for a wireless, mm-scale system that can be implanted through minimally invasive procedures. Recent PNS research has focused on the development of small volume, battery-less systems that are capable of safe and efficient power transfer centimeters into tissue [2]–[4]. Typically, PNSs only require a single electrode pair to stimulate the nerve. Recently, ultrasound has been proposed as an efficient way to power and communicate with mm-scale implants in deep tissue, resulting in significant volume reduction [2], [3]. Compared to RF at 2GHz, ultrasound energy at 2MHz has less attenuation through tissue (1dB/cm vs. 3dB/cm), a higher FDA limit (7.2mW/mm^2 vs. 0.1mW/mm^2), and smaller wavelength (0.75mm vs. 25mm) [1].

We present a 10mg, 6.5mm^3 peripheral nerve stimulator that uses a single piezocrystal for power and bidirectional communication with ultrasound, and efficiently converts received power to provide well-controlled stimulation to the nerve. The smallest volume stimulators [3], [4] have been implemented with passive components, providing inefficient voltage-mode stimulation that is sensitive to received power and electrode impedance. Active, multi-channel neurostimulators utilizing inductive coupling have achieved high efficiencies [5], [6], but require cm-scale coils and occupy larger volumes. This work scales down the volume of the implant by using a single piezocrystal coupled to an IC and wireless protocol that achieves high efficiency and precision. High efficiency is achieved through a combination of protocol design, duty cycling, active rectification, and reducing the need for high voltage compliance stimulation. For precision, the stimulation IC utilizes a current-mode stimulator to deliver a well-controlled charge independent of electrode size and impedance, which can be highly variable at small scales. The stimulation waveform is dynamically reconfigurable via the structure of the input ultrasound, rather than bit packets. The protocol enables sub-μs temporal precision of the stimulation waveform without the need for a clock, and an inherently high dynamic range of pulse widths and frequencies (e.g. f_{stim} = 0-2kHz), while minimizing complexity and therefore power.

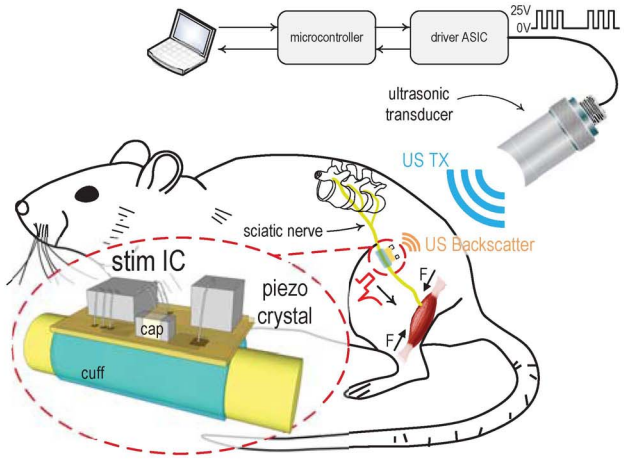

Fig. 1. System illustration of the implantable device. The implant is wirelessly powered via harvested ultrasound from a piezo crystal. By detecting the envelope of incoming ultrasound, the stimulation IC dynamically reconfigures stimulation pulse width, pulse interval, interphase gap, and amplitude.

II. System Architecture

Fig. 1 depicts the system concept. The implanted stimulation mote is cuffed to a peripheral (e.g. sciatic) nerve while an external transducer powers and controls the mote with ultrasound. The external transducer is driven by a custom ASIC that level-shifts the microcontroller-generated ultrasound transmit signal [7]. The maximum drive voltage of the ex-

978-1-5386-2483-8/18/$31.00 ©2018 IEEE

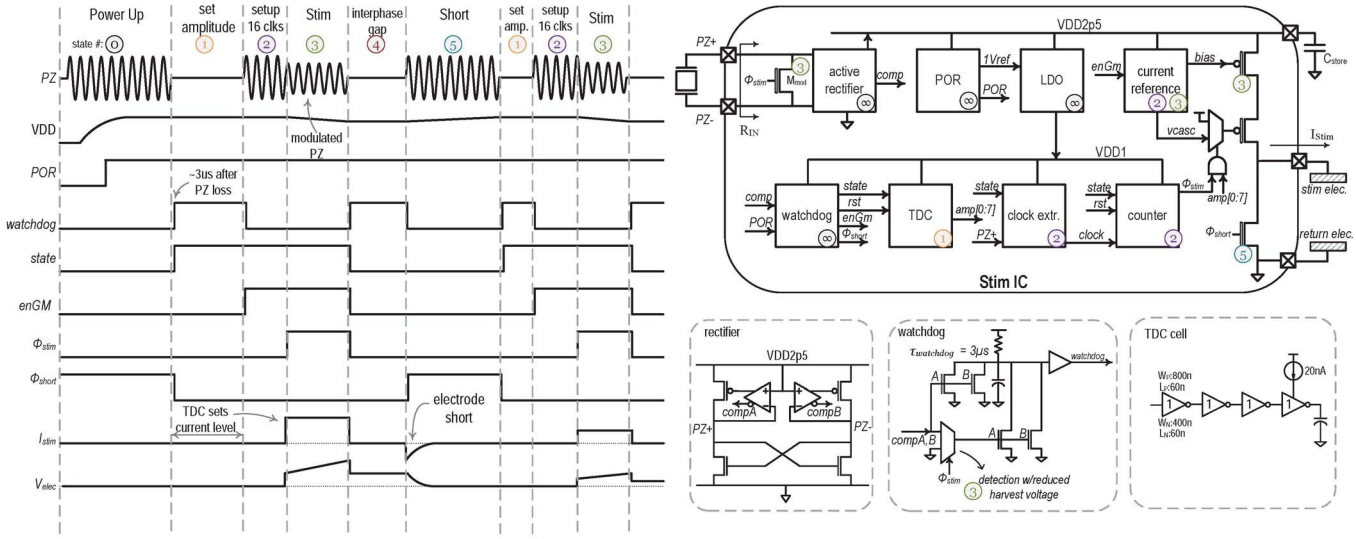

Fig. 2. Timing diagram with resulting stimulation waveforms and system architecture. The numbers indicate the state when a subcircuit is active.

ternal transducer in this implementation is 32V, resulting in $\sim$350μW maximum received power in the implant. Depending on protocol, stimulation powers can match or even exceed this value, making conversion efficiency from received power to stimulation power essential. The implanted mote consists of the stimulation IC, a piezocrystal, and a charge storage capacitor mounted on a flexible PCB with two electrodes on the bottom side. The incident ultrasound wave is reflected back to the external transducer with a magnitude related to the electrical load impedance seen by the piezo. This load impedance is modulated by the stimulation IC to provide a single bit that indicates chip state (stimulation on or off), for safety.

The protocol utilizes edge-detection to encode for timing, rather than clocks, which reduces power consumption while simultaneously provides a high degree of timing control and precision. As shown in the timing diagram of Fig. 2, an initial power-up sequence charges the implants storage capacitor and a POR signal initializes the system. A watchdog timer is used to detect ultrasound-free intervals (UFIs) in the incoming ultrasound. For every UFI, the stimulation state is toggled. The first UFI length encodes the stimulation amplitude, which is decoded with a 3-bit TDC. The next burst of ultrasound generates the stimulation command; a 16-clock cycle header generates a delay to allow bias circuitry to settle prior to stimulation. After the header, the stimulation current source and the modulation switch (for backscattering) are enabled. A single bit is backscattered in this phase to indicate whether or not the mote is stimulating as a safety indication. A second UFI encodes the interphase gap, a feature shown to have an impact on stimulation thresholds. The next ultrasound burst enables a shorting phase that clears accumulated charge from the stimulation electrode. Since high capacity stimulation discharges the storage capacitor, this phase is also used for recharging the capacitor.

Fig. 2 also shows the architecture of the IC. The switch M_{mod} changes the impedance from $\sim$100kΩ to $\sim$4kΩ at the piezo terminals for backscatter. The impedance change is sufficient to serve as a 1-bit indicator flag (measurement shown in Fig. 6), while allowing all circuits on the IC to function normally under reduced voltage conditions. For efficiency, an active full-wave rectifier converts the piezo voltage (3V-5V) to a nominal 2.5V supply. An LDO regulates a 1V supply for the digital control circuitry. The rectifier comparator outputs are also used to drive the watchdog switches. The sensitivity of the watchdog is increased during stimulation using low-voltage devices to account for the reduced voltage at the piezo terminals. The TDC consists of 8 current-starved inverter delay stages to generate a 3-bit amplitude code. The unit delay is designed to be greater than twice the watchdog time constant to be insensitive to piezo ring-down as well as process variations controlling the watchdog time constant, which is set by an RC. To further conserve power, most subcircuits are heavily duty-cycled, where corresponding numbers in Fig. 2 indicate the phase when a particular subcircuit is active. For example, the clock extractor is only active to generate the 16-cycle header, which ensures proper settling of the constant-gm current reference.

III. System Characterization

The IC is fabricated in TSMC 65nm LP-CMOS process and occupies an area of 1mm^2 (Fig. 3). The active area is 150x400μm^2. Fig. 3 also shows the mote assembly, which measures 2x3.25x1mm^3 and 10mg. The height is dominated by the 750μm tall piezo and wire bond on a 100μm-thick polyimide PCB. A 4μF 0201 surface mount capacitor is used to store energy for high-capacity stimulation. A 10μm-thick conformal layer of parylene is used to encapsulate the entire mote. A thin encapsulation layer ensures good acoustical transmission between the surrounding tissue and the piezo. The back of the mote features two 550x550μm^2 Au electrodes (stim and return) electroplated with PEDOT:PSS. The PEDOT:PSS coating reduces the electrode impedance several orders of magnitude at low frequency, reducing the

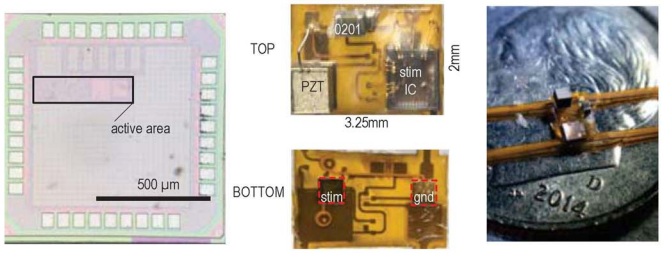

Fig. 3. Die microphotograph and board photographs.

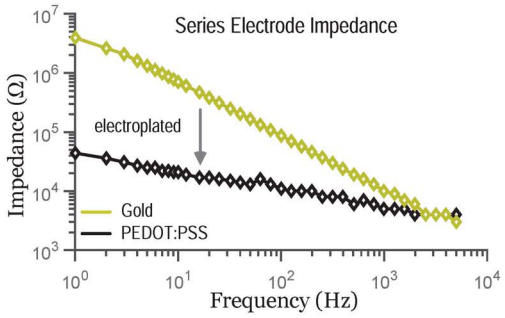

Fig. 4. Impedance measurement of the electrodes in series before and after electroplating.

required stimulation headroom and eliminating the need for high voltage circuits, improving chip efficiency (Fig. 4). Furthermore, a lower supply voltage enables the use of higher density capacitors with lower voltage ratings.

Fig. 5 shows the measured output current versus UFI-length and the chip efficiency. While the relative error between current levels of the DAC or TDC steps is small, the absolute error will be sensitive to process variation. However, this is easily calibrated by adjusting the protocol with the external system. The overall chip efficiency (η) is defined as the stimulation output power divided by the input power to the chip (82% at $I_{Stim,AVG}$ = 48μA). The average stimulation current is defined as $I_{Stim,AVG} = I_{Stim,AMP}{*}T_{Pulse}{*}F_{Stim}$. When not stimulating, the DC power is measured to be 4μW. When stimulating, the total power dissipation is roughly $P_{TOT} = 2.5V{*}I_{Stim,AVG}/\eta$. Since implants are typically limited by the amount of available power, the design is optimized for high efficiency for higher capacity stimulation.

In order to discriminate between shorting and stimulation states at an external reader, the modulation switch ensures a significant change in impedance. Backscatter amplitude is modulated by the electrical impedance load on the piezo (chip R_{IN}; changes with chip load). The impedance of the modulation switch is designed to approximate the series resonant resistance of the piezo, where the backscatter profile is most sensitive to small change (Fig. 6). This allows for reader to distinguish between states even at a high load. The expected backscatter profile was simulated with a finite element method.

Fig. 7 shows *in vitro* results of the stimulation mote powered and controlled via ultrasound near 1.85MHz, the piezo resonant frequency. The mote was suspended in ultrasound gel at the focal length of the external transducer (21.5mm). The transient results demonstrate the mote executing two different

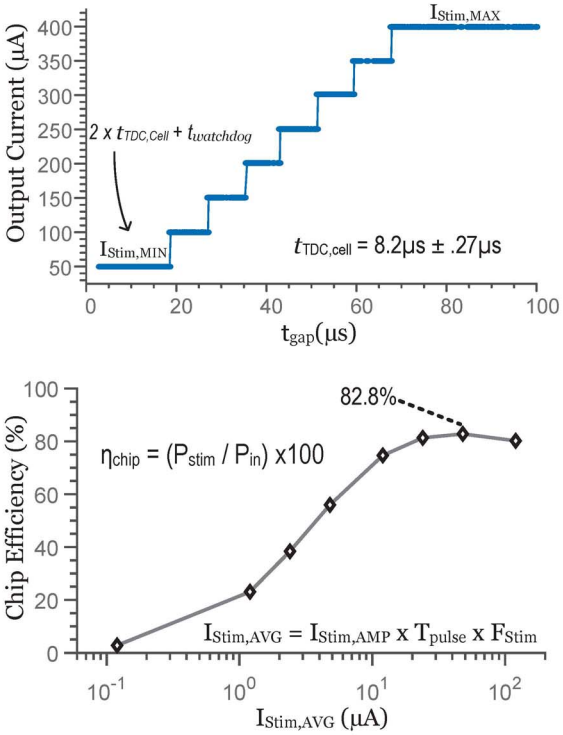

Fig. 5. Stimulator output current plotted against TDC time and overall chip efficiency.

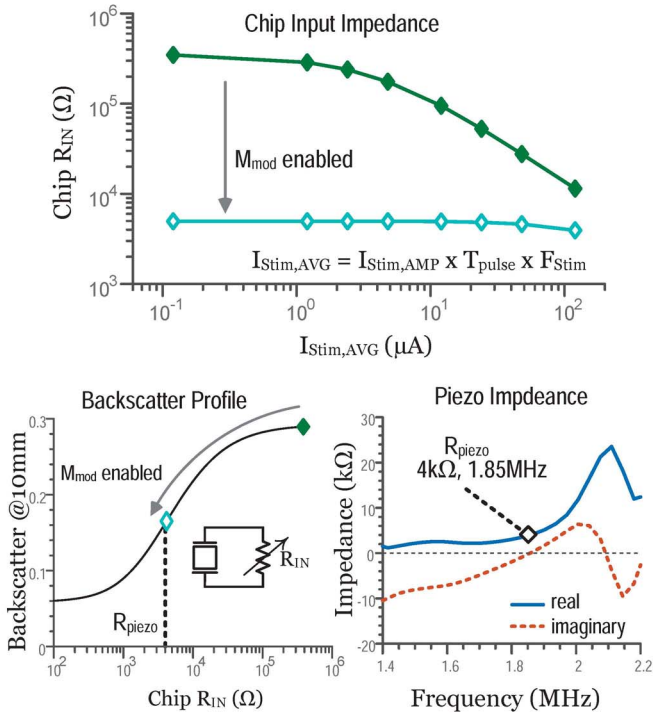

Fig. 6. Measured chip input resistance versus stimulation load. Plot of the estimated backscatter profile based on measured chip input resistance and piezo impedance.

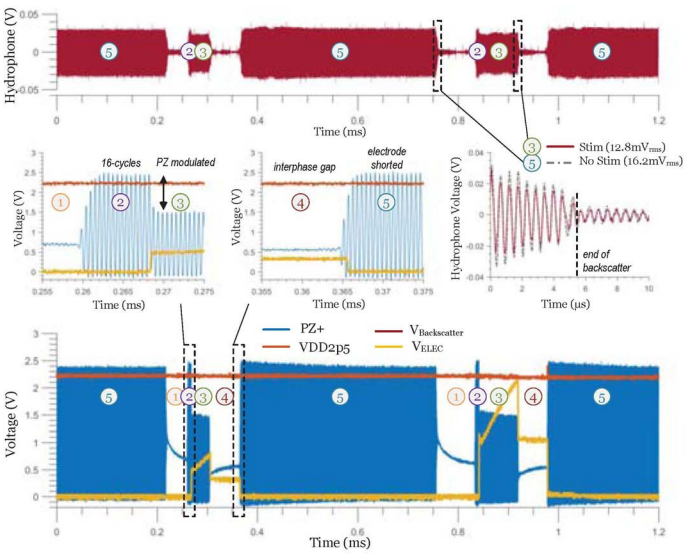

Fig. 7. Mote suspended in ultrasound gel powered via ultrasound with an external transducer and simultaneously recorded backscatter using a hydrophone. (electrode model: R_{ELEC} = 2.2kΩ, C_{ELEC} = 22nF)

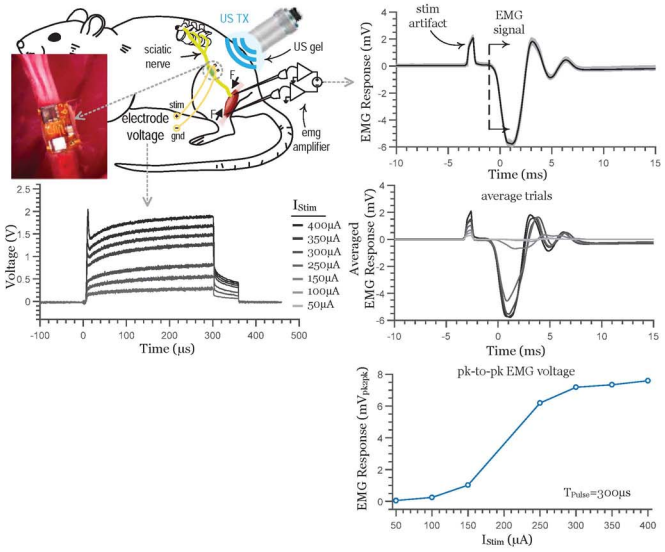

Fig. 8. *In vivo* validation of the implant. The plots show the measured voltage across the electrodes during stimulation and EMG response vs. stimulation amplitude.

stimulation parameters as a function of the input ultrasound. Backscattered ultrasound is measured at the end of shorting and stimulation phases (when free of acoustical feedthrough) using a second external hydrophone, providing a wireless single-bit indicator of the chips current state.

IV. In Vivo Measurements

To validate the mote *in vivo*, the device was cuffed to the sciatic nerve of an anesthetized rodent (Fig. 8) at a depth of 21.5mm. All *in vivo* experiments were performed in compliance with the NIH Guide for the Care and Use of Laboratory Animals. Needle electrodes were inserted in the contracting muscle and motor unit potentials were recorded differentially. Test leads were used to monitor the electrode voltage as a function of time to demonstrate the delivery of stimulation current. Stimulation amplitude was swept to create intramuscular EMG recruitment curves that are consistent with established physiological measurements and demonstrates that the mote can deliver the full range of nerve activation intensities.

V. Conclusion

We compare against recently published implantable small-volume and high-efficiency optical and electrical neurostimulators [3]–[6] in Table I. To our knowledge, this work achieves highest efficiency (82%) at the smallest volume (6.5mm^3) and mass (10mg), with the fewest external components, improving the FOM, defined as volume over efficiency, by 3.5x over state-of-the-art while delivering well-controlled stimulation capable of full-scale activation of a rodent sciatic nerve *in vivo*.

Table I.

	BioWireless '16	Nat. Methods '15	ISSCC '14	ISSCC '16	**This work**
Stim. type	optical	optical	voltage	current	**current**
Link	ultrasound	RF	inductive	inductive	**ultrasound**
$f_{carrier}$ [MHz]	0.955	1500	--	2	**1.85**
Process [nm]	discrete	discrete	350	180HV	**65**
No. of Stimulators	1	1	4	40	**1**
F_{Stim} [Hz]	--	--	7.6 - 244	<20k	**0 - 2k+**
T_{Pulse} resolution [us]	continuous	continuous	16	10	**continuous**
$I_{Stim,max}$ [µA]/ resol. [bit]	undefined	undefined	voltage mode	500 / 5b	**400 / 3b**
$depth_{tx-rx}$ [mm]	60	30	10	--	**21.5**
No. of ext. components	6 + piezo	8 + coil	9 + coil	6 + 2 coils	**1 + piezo**
Packaged	Yes	Yes	No	Yes	**Yes**
Mass [mg]	--	20 - 50	--	700	**10**
Efficiency (P_{stim}/P_{in}) [%]	76	33.3*	80.4	--	**82**
Volume [mm^3]	21.6	10 - 25	--	500	**6.5**
FOM (Volume/Efficiency)	0.28	0.3 - 0.75	--	--	**0.079**

*estimated

Acknowledgment

This work was supported by NSF EAGER and the sponsors of BWRC.

References

[1] D. Seo, J. M. Carmena, J. M. Rabaey, E. Alon, and M. M. Maharbiz, "Neural dust: an ultrasonic, low power solution for chronic brain-machine interface," arXiv:1307:2196. http://arxiv.org/abs/1307.2196

[2] D. Seo, R. M. Neely, K. Shen, U. Singhal, E. Alon, J.M. Rabaey, J.M. Carmena, and M. M. Maharbiz, "Wireless recording in the peripheral nervous system with ultrasonic neural dust," *Neuron* vol. 91, pp. 529–539, 2016.

[3] M. Weber, A. Bhat, T. C. Chang, J. Charthad, and A. Arbabian, "A miniaturized ultrasonically powered programmable optogenetic implant stimulator system," *IEEE Topical Conference on Biomedical Wireless Technologies, Networks, and Sensing Systems (BioWireleSS)*, April 2016.

[4] K. Montgomery, A. J. Yeh, J. S. Ho, V. Tsao, S. Mohan Iyer, L. Grosenick, E. A. Ferenczi, Y. Tanabe, K. Deisseroth, S. L. Delp, and A. S. Poon, "Wirelessly powered, fully internal optogenetics for brain, spinal, and peripheral circuits in mice," *Nat Methods*, vol. 10, pp. 969–974, 2015.

[5] Y. K. Lo, C. W. Chang, Y. C. Kuan, S. Culaclii, B. Kim, K. Chen, P. Gad, V. R. Edgerton, and W. Liu, "A 176-Channel 0.5cm^3 0.7g Wireless Implant for Motor Function Recovery after Spinal Cord Injury," *ISSCC Dig. Tech. Papers*, pp. 382–383, Jan. 2016

[6] H. M. Lee, K. Y. Kwon, W. Li, and M. Ghovanloo, "A power-efficient switched-capacitor stimulating system for electrical/optical deep brain stimulation," *IEEE J. Solid-State Circuits*, vol. 50, pp. 360–374, Jan. 2015.

[7] D. K. Piech, J. E. Kay, B. E. Boser, and M. M. Maharbiz, "Rodent wearable ultrasound system for wireless neural recording," *2017 39th Annual International Conference of the IEEE Engineering in Medicine and Biology Society (EMBC)*, pp. 221–225, July 2017.